



Quantification of tropical monsoon precipitation changes in terms of interhemispheric differences in stratospheric sulfate aerosol optical depth

Shinto Roose^{1,2} · Govindasamy Bala¹ · K. S. Krishnamohan³ · Long Cao⁴ · Ken Caldeira⁵

Received: 25 August 2022 / Accepted: 16 April 2023
© The Author(s) 2023

Abstract

Stratospheric Aerosol Geoengineering (SAG) is one of the solar geoengineering approaches that have been proposed to offset some of the impacts of anthropogenic climate change. Past studies have shown that SAG may have adverse impacts on the global hydrological cycle. Using a climate model, we quantify the sensitivity of the tropical monsoon precipitation to the meridional distribution of volcanic sulfate aerosols prescribed in the stratosphere in terms of the changes in aerosol optical depth (AOD). In our experiments, large changes in summer monsoon precipitation in the tropical monsoon regions are simulated, especially over the Indian region, in association with meridional shifts in the location of the intertropical convergence zone (ITCZ) caused by changes in interhemispheric AOD differences. Based on our simulations, we estimate a sensitivity of $-1.8^{\circ} \pm 0.0^{\circ}$ meridional shift in global mean ITCZ and a $6.9 \pm 0.4\%$ reduction in northern hemisphere (NH) monsoon index (NHMI; summer monsoon precipitation over NH monsoon regions) per 0.1 interhemispheric AOD difference (NH minus southern hemisphere). We also quantify this sensitivity in terms of interhemispheric differences in effective radiative forcing and interhemispheric temperature differences: $3.5 \pm 0.3\%$ change in NHMI per unit (Wm^{-2}) interhemispheric radiative forcing difference and $5.9 \pm 0.4\%$ change per unit ($^{\circ}\text{C}$) interhemispheric temperature difference. Similar sensitivity estimates are also made for the Indian monsoon precipitation. The establishment of the relationship between interhemispheric AOD (or radiative forcing) differences and ITCZ shift as discussed in this paper will further facilitate and simplify our understanding of the effects of SAG on tropical monsoon rainfall.

Keywords Stratospheric Aerosol Geoengineering (SAG) · Northern Hemispheric monsoon index (NHMI) · Indian summer monsoon · Interhemispheric difference in aerosol optical depth (AOD)

1 Introduction

Anthropogenic activities such as emissions of greenhouse gases and land-use changes have led to an increase in global mean temperature by 1.1°C during 2011–2020 relative to the pre-industrial period, and climate change projections show that the warming may exceed 1.5°C within the next few decades (IPCC 2021a, b). Rapid reductions in greenhouse emissions can potentially reduce the amount of future warming. However, emission reductions may take decades and act slowly to reduce global warming. In this context, a set of solar geoengineering approaches (Caldeira et al. 2013), which aims to cool the Earth by reflecting more sunlight to space, has been proposed to offset some impacts of anthropogenic global warming (Keith and Dowlatabadi 1992; Irvine et al. 2019). Solar geoengineering approaches are estimated to be generally less expensive than the cost

✉ Shinto Roose
thejusshinto@gmail.com

¹ Centre for Atmospheric and Oceanic Sciences, Indian Institute of Science, Bangalore 560012, India

² Present Address: Department of Civil Engineering, McGill University, Montreal, Quebec, Canada

³ School of Environmental Studies, Cochin University of Science and Technology, Cochin 682022, India

⁴ Department of Atmospheric Sciences, School of Earth Sciences, Zhejiang University, Hangzhou 310027, Zhejiang, People's Republic of China

⁵ Department of Global Ecology, Carnegie Institution for Science, Stanford, CA 94305, USA

associated with emission reductions (Keith et al. 2010). However, solar geoengineering does not alleviate other ecosystem stressors, such as ocean acidification (Tilmes et al. 2020; Jin et al. 2022).

A deliberate injection of sulfate aerosols into the stratosphere (Budyko 1977; Crutzen 2006; Wigley 2006; Svoboda et al. 2011), termed Stratospheric Aerosol Geoengineering (SAG) is one of the most feasible solar geoengineering approaches (Keith et al. 2010; Mahajan et al. 2019; Aldy et al. 2021). However, SAG could lead to unintended consequences which may affect the planet in adverse ways (e.g., Kravitz and MacMartin 2020). For example, there is scientific consensus that the deliberate alteration of solar radiation to cool the planet would affect the global water cycle (Bala et al. 2008; Tilmes et al. 2013) and impact regional monsoons (Robock et al. 2008; Nalam et al. 2018; Zhao et al. 2021; Krishnamohan and Bala 2022).

Past studies indicate large uncertainties in climate system response to SAG. One of the uncertainties is related to the climate's response to meridional profiles of insolation reduction (Lutsko et al. 2020; Ban-Weiss and Caldeira 2010; Modak and Bala 2014; Nalam et al. 2018) which would depend on the choice of injection location (Tilmes et al. 2017). Hemispherically asymmetric forcing from stratospheric sulfate aerosols would create an interhemispheric temperature gradient, which would lead to shifts in the mean latitudinal position of the intertropical convergence zone (ITCZ) (Schneider et al. 2014; Haywood et al. 2013; Smyth et al. 2017; Cheng et al. 2022). The shift in the location of ITCZ is a major factor in the tropical monsoon variability (Fleitmann et al. 2007; Berry and Reeder 2014; Hari et al. 2020). For instance, observations show that an increase in aerosol loading due to large volcanic eruptions in one hemisphere reduces the monsoon precipitation in the same hemisphere (Liu et al. 2016). In a modeling study, Nalam et al. (2018) have shown that an introduction of stratospheric sulfate aerosol loading over the Arctic creates a southward shift in ITCZ and weakens the northern hemisphere (NH) monsoons, but enhances the southern hemisphere (SH) monsoons. In general, the summer monsoon precipitation decreases in the hemisphere where sulfate aerosols are injected but increases in the opposite hemisphere, which is linked to the changes in interhemispheric surface temperature contrast and shifts in the location of ITCZ (Krishnamohan and Bala 2022). This sensitivity of monsoon precipitation to the asymmetry in aerosol forcing between the hemispheres is consistent with the recent Intergovernmental Panel on Climate Change (IPCC) assessment that the decline in global land monsoon precipitation from the 1950s to the 1980s are partly attributed to anthropogenic NH aerosol emissions (IPCC 2021b SPM).

The SAG-induced surface cooling and heating in the stratospheric sulfate aerosol layer could also alter the

tropical vertical temperature profile, weakening the tropical overturning circulation, suppressing convection and consequently weakening tropical-mean precipitation (Ferraro et al. 2014). This is because the SAG-induced surface cooling and upper-tropospheric/lower stratospheric radiative heating could produce atmospheric stabilization with reduction in the tropospheric turbulence and updraft velocities (Visioni et al. 2018). Thus, SAG could alter the global-mean and regional precipitation because of stratospheric warming due to the absorption of shortwave and longwave radiations by the aerosols (Ferraro et al. 2011, 2014; Simpson et al. 2019) and because of shifts in the location of ITCZ induced by the changes in interhemispheric temperature gradient (Haywood et al. 2013; Smyth et al. 2017; Nalam et al. 2018; Zhao et al. 2021; Krishnamohan and Bala 2022). Recent studies have shown that optimized simultaneous injection at multiple locations can achieve multiple temperature targets simultaneously. Such simultaneous injections at multiple latitudes could offset the changes in interhemispheric temperature gradient and equator to pole temperature gradient in addition to offsetting the CO₂-induced global mean temperature (MacMartin et al. 2017; Kravitz et al. 2017, 2019; Tilmes et al. 2018; Richter et al. 2018).

Our objective in this paper is to quantify the sensitivity of precipitation in the tropical monsoon regions to the latitudinal distribution of prescribed sulfate aerosols, in terms of the change in interhemispheric aerosol optical depth (AOD) differences. Earlier studies have quantified the ITCZ shifts in terms of the interhemispheric temperature differences (Nalam et al. 2018; Krishnamohan and Bala 2022) or interhemispheric tropical temperature differences (Zhao et al. 2021). As changes in both interhemispheric temperature differences and ITCZ shifts represent the response to the introduced climate forcing, the relation between changes in interhemispheric temperature difference and the shifts in the latitudinal position of ITCZ is only an “association”. By relating the ITCZ shift to the changes in interhemispheric AOD differences or interhemispheric radiative forcing differences, we attempt to relate the cause (interhemispheric AOD or radiative forcing difference) to the effect (ITCZ shift). We believe that the establishment of the relationship between AOD (or radiative forcing) and ITCZ shift would further facilitate and simplify our understanding of the effects of SAG on tropical monsoon rainfall.

Past studies Modak and Bala (2014) and Nalam et al. (2018) have examined the global mean and summer monsoon precipitation response to idealized background sulfate aerosols (size < 0.1 μm) in the stratosphere, which are formed by the transport of natural and anthropogenic sulfur-containing compounds from the troposphere (Rasch et al. 2008). In this study, we analyze the monsoon responses to idealized sulfate aerosols with sizes typical of those produced by volcanoes (~0.4 μm) which are relevant to the SAG

problem. Volcanic type aerosols are formed 6–12 months after a volcanic eruption (Stenchikov et al. 1998; Rasch et al. 2008) and are more efficient in cooling the climate when they are prescribed higher in the stratosphere (Krishnamohan et al. 2019).

Our simulations are similar to a recent study by Zhao et al. (2021), in which different meridional distributions of volcanic type sulfate aerosols are prescribed in the stratosphere to offset CO₂-induced changes in global mean temperature. Zhao et al. (2021) studied the impact of varying meridional profiles of sulfate aerosols (as represented by Ban-Weiss and Caldeira 2010) on the global mean temperature and precipitation changes and the global mean ITCZ shifts. However, their analysis does not extend to global and regional monsoon precipitation changes. In this paper, we extend the investigation of Zhao et al. (2021) to quantify the sensitivity of tropical monsoon precipitation changes to unit changes in interhemispheric AOD and radiative forcing differences. We also analyze in detail the changes in summer monsoon precipitation over the country, India.

2 Model and experimental design

In this study, our simulations are performed using the NCAR Community Earth System Model version 1.0.4. (Gent et al. 2011). We use the model configuration in which the atmospheric component (Community Atmosphere Model version 4—CAM4 with a horizontal resolution of 1.9° × 2.5° (latitude × longitude) and 26 hybrid sigma-pressure vertical layers; Neale et al. 2010) is coupled to a land model (Community Land Model version 4; Oleson et al. 2010), sea ice (Community Ice Code version 4; Bailey et al. 2010) and a slab ocean.

A present-day experiment, called 1 × CO₂, with atmospheric CO₂ concentration corresponding to present-day (400 ppm) and another experiment (2 × CO₂) where the CO₂ concentration is doubled (800 ppm, control run) are performed. Following previous studies Ban-Weiss and Caldeira (2010), Modak and Bala (2014) and Zhao et al. (2021), we perform a set of SAG experiments with varying meridional distribution of sulfate aerosols (Fig. 1a). The meridional profiles of aerosol concentration are functions of Legendre polynomials in the sine of latitude. In our SAG experiments, aerosols are added to the climate state where the present-day atmospheric CO₂ concentration (400 ppm) is doubled (2 × CO₂). We use both prescribed-SST and slab ocean configurations of the model in this study. In CAM4, smaller-size background aerosols can absorb water and grow larger depending on the relative humidity at a given location (Krishnamohan et al. 2020). Large volcanic aerosols in the model are assumed to contain constant fractional amount of water: a fixed composition of 75% sulfuric acid and 25%

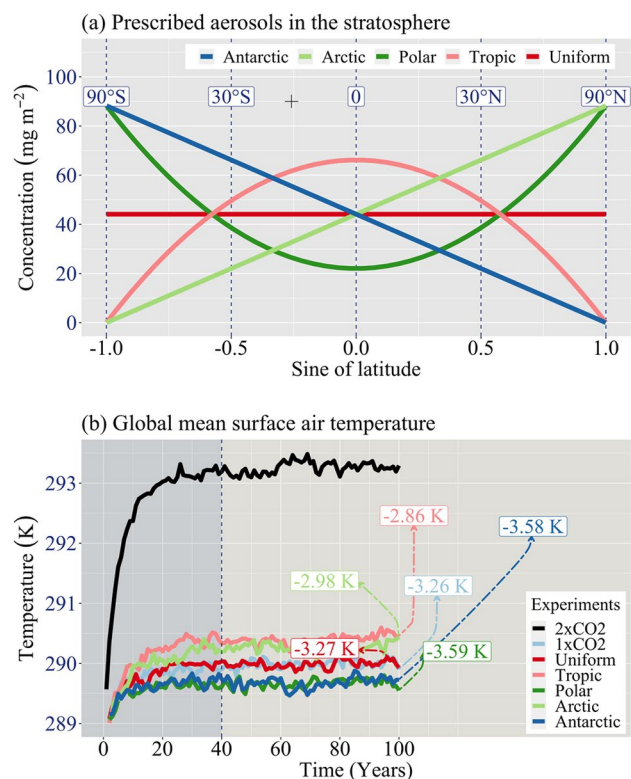


Fig. 1 **a** Meridional distribution of zonal mean concentration of volcanic sulfate aerosols prescribed in the stratosphere (at 37 hPa) and **b** the time series of the global-mean annual surface temperature in the 100-year slab-ocean simulations. The total amount of aerosols is 22.5 Mt in all experiments. The global annual mean change in surface temperature in each experiment relative to the 2 × CO₂ climate simulation in the last 60-years is also shown in **b**

water (Neale et al. 2010; Ammann et al. 2003). Relative to the smaller background aerosols, volcanic aerosols cause more warming in the stratosphere as they have a larger cross section for absorption compared to the background aerosols (Krishnamohan et al. 2019). By default, CAM4 has 0.6 Mt of background aerosols in the form of ammonium sulfate in the stratosphere (Nalam et al. 2018).

The five SAG experiments conducted for this study are (see Text S1): (1) uniform case, which is similar to the 2 × CO₂ experiment, but an additional amount of 22.5 Mt of volcanic sulfate aerosols are prescribed in the stratosphere (37 hPa) and distributed uniformly around the globe, (2) Arctic case in which the prescribed aerosol is distributed linearly from the South to the North Pole with a maximum concentration at the North Pole, (3) Antarctic case in which the aerosol concentration increases linearly from the North to the South Pole with a maximum concentration at the South Pole, (4) Polar case in which the maximum concentration of aerosols are at the poles and the minimum is at the equator, and (5) Tropic case in which the total prescribed concentration is maximum at the equator and minimum at the poles

(Fig. 1a). For all SAG simulations with prescribed aerosol concentration, complex aerosol processes such as aerosol microphysics, aerosol chemistry, transport and sedimentation are not modeled. All seven experiments are conducted in both prescribed-SST and slab ocean configurations. Prescribed-SST simulations are conducted for 60 years and data from last 30 years is used to compute the effective radiative forcing, which is represented by the net radiative flux change at the top of the atmosphere (Hansen et al. 1997). In the case of slab ocean simulations, last 60 years of data from 100-year simulations are used for the analysis.

3 Results and discussion

Zhao et al. (2021) have investigated the effects of varying meridional profiles of sulfate aerosols on the global mean temperature and precipitation changes, climate sensitivity, global mean ITCZ shifts and changes in cross equatorial heat transport. As discussed earlier, we have used the same meridional distribution of sulfate aerosols (Fig. 1a) as in Zhao et al. (2021). In this study, we extend the investigation of Zhao et al. (2021) by focusing on the effects of varying meridional profiles of sulfate aerosols on the tropical monsoon precipitation after a brief discussion of radiative forcing and temperature and precipitation changes.

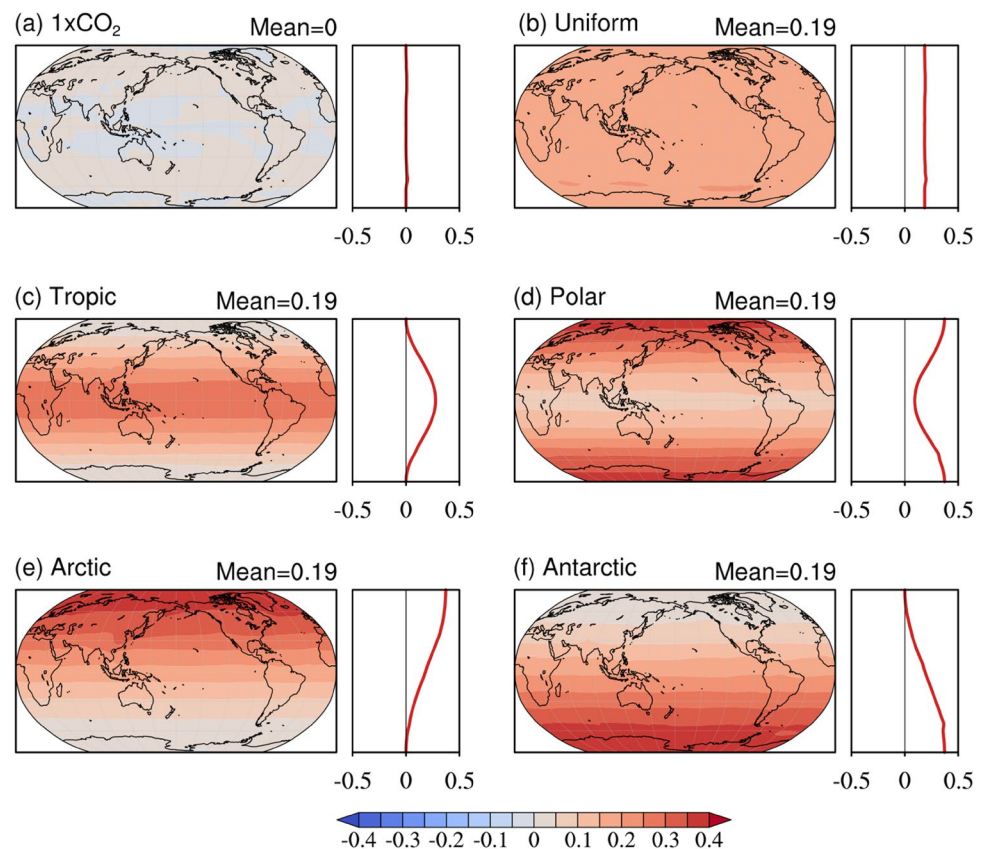
3.1 Aerosol optical depth and radiative forcing

The spatial patterns of additional AOD associated with different meridional distributions of volcanic sulfate aerosols (Fig. 1a) in our simulations are shown in Fig. 2. The spatial patterns of AOD indicate that the aerosols are distributed uniformly in the zonal direction. Large gradients can be seen in meridional direction (Figs. 2). The additional sulfate aerosols prescribed in our SAG experiments (Fig. 1a) cause an increase in global mean AOD by ~ 0.2 (Fig. 2) and nearly offset the warming by doubling of CO_2 concentration (Fig. 1b).

In this study, we use the effective radiative forcing (ERF, Hansen et al. 1997; Hansen et al. 2005; Myhre et al. 2013) as a measure for imposed radiative forcing. ERF is estimated as the change in net radiative flux at the top of the atmosphere after the stratosphere, troposphere and land surface have adjusted to the imposed forcing in the prescribed-SST simulations (Duan et al. 2018; Modak et al. 2018; Krishnamohan et al. 2019; Zhao et al. 2021). ERF is estimated using the equations shown in SI Equations. Previous studies show that the magnitude of global mean surface temperature scales linearly with ERF (Forster et al. 2021).

The ERF in the Uniform, Tropic, Polar, Arctic, and Antarctic cases, relative to the $2 \times \text{CO}_2$ simulation, is -4.6 ± 0.1 , -5.0 ± 0.0 , -4.1 ± 0.0 , -4.5 ± 0.1 and $-4.4 \pm 0.0 \text{ Wm}^{-2}$, respectively (Fig. S1), indicating that the magnitude of ERF

Fig. 2 The spatial pattern of aerosol optical depth (AOD) in the $1 \times \text{CO}_2$ simulation and in the five stratospheric geoengineering experiments relative to the $2 \times \text{CO}_2$ simulation. The changes in global mean AOD are shown in the top right of the panels. The subpanel on the right of each panel shows the zonal mean changes



is largest, given a fixed total amount, when aerosols are placed in the tropical stratosphere (Modak and Bala 2014). This is because of the latitudinal distribution of incoming solar radiation which has a maximum in the tropics. Meridionally varying sulfate aerosol loading (Fig. 1a) generate large hemispherical asymmetries in sulfate AOD (Fig. 2). In our simulations, we find that the interhemispheric AOD difference and ERF show strong correlation with a linear regression coefficient of $\sim 2 \text{ Wm}^{-2}$ per 0.1 interhemispheric AOD difference (Fig. 3a).

The interhemispheric AOD differences associated with asymmetric aerosol loading about the equator in the Arctic and Antarctic cases lead to large interhemispheric radiative forcing difference of, respectively, -3.7 ± 0.1 and $3.6 \pm 0.1 \text{ Wm}^{-2}$ (Fig. 3a). However, in the cases with hemispherically symmetric aerosol loading (Uniform, Tropic and Polar cases), the interhemispheric ERF differences are very small (-0.1 ± 0.1 , 0.2 ± 0.1 and $-0.1 \pm 0.1 \text{ Wm}^{-2}$) as there is no interhemispheric AOD difference.

3.2 Global temperature and precipitation response

In our simulations, the doubling of atmospheric CO_2 concentration from its present-day level of 400 ppm in the $1 \times \text{CO}_2$ simulation to 800 ppm in the $2 \times \text{CO}_2$ simulation causes an increase in global mean ERF magnitude of $\sim 4 \text{ Wm}^{-2}$ (Fig. S1) at the top of the atmosphere and an increase in global mean surface temperature by $3.3 \pm 0.0 \text{ K}$ (Fig. 4a).

The SAG experiment, Uniform case with spatially uniform stratospheric sulfate AOD values (Fig. 2) has a negative radiative forcing of $-4.6 \pm 0.1 \text{ Wm}^{-2}$ (Fig. S1) and offsets the global mean warming of $\sim 3.3 \pm 0.0 \text{ K}$ due to the doubling of CO_2 (Fig. 4b). The Tropic and Polar cases have negative radiative forcing of -5.0 ± 0.0 and $-4.1 \pm 0.0 \text{ Wm}^{-2}$, respectively (Fig. S1), and simulate a reduction in global mean surface temperature by $2.9 \pm 0.0 \text{ K}$ and $3.6 \pm 0.0 \text{ K}$, respectively (Fig. 4). The global mean surface cooling simulated in the Arctic and Antarctic cases is $3.0 \pm 0.0 \text{ K}$ and $3.6 \pm 0.0 \text{ K}$, respectively (Fig. 4). Out of the five SAG experiments, the Polar and Tropic cases simulate the maximum and minimum cooling in global mean surface temperatures, respectively (Fig. 4). These results are consistent with Zhao et al. (2021), and contrary to the results from Modak and Bala (2014), which show that higher aerosol concentration in the tropics leads to more cooling than in the Polar case. Zhao et al. (2021) attributes these changes to different generations of the CAM model used in these two studies. Modak and Bala (2014) used version 3 of CAM (CAM3), whereas this study and Zhao et al. (2021) use CAM4. It is likely that the use of different meridional profiles of aerosols also contributes to the differences in results presented here and Modak and Bala (2014).

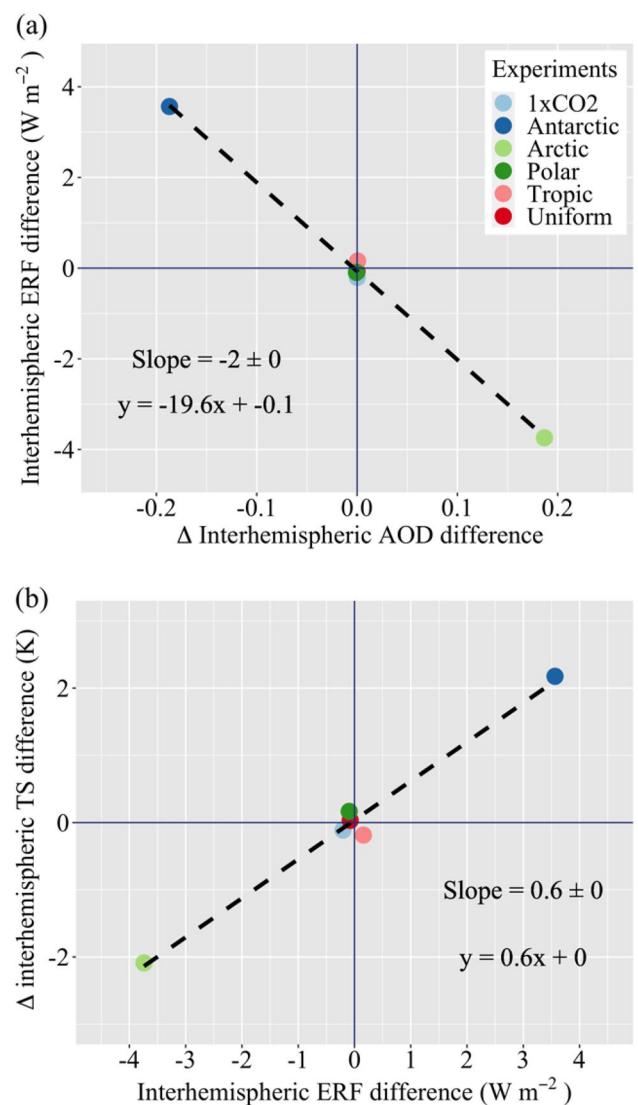
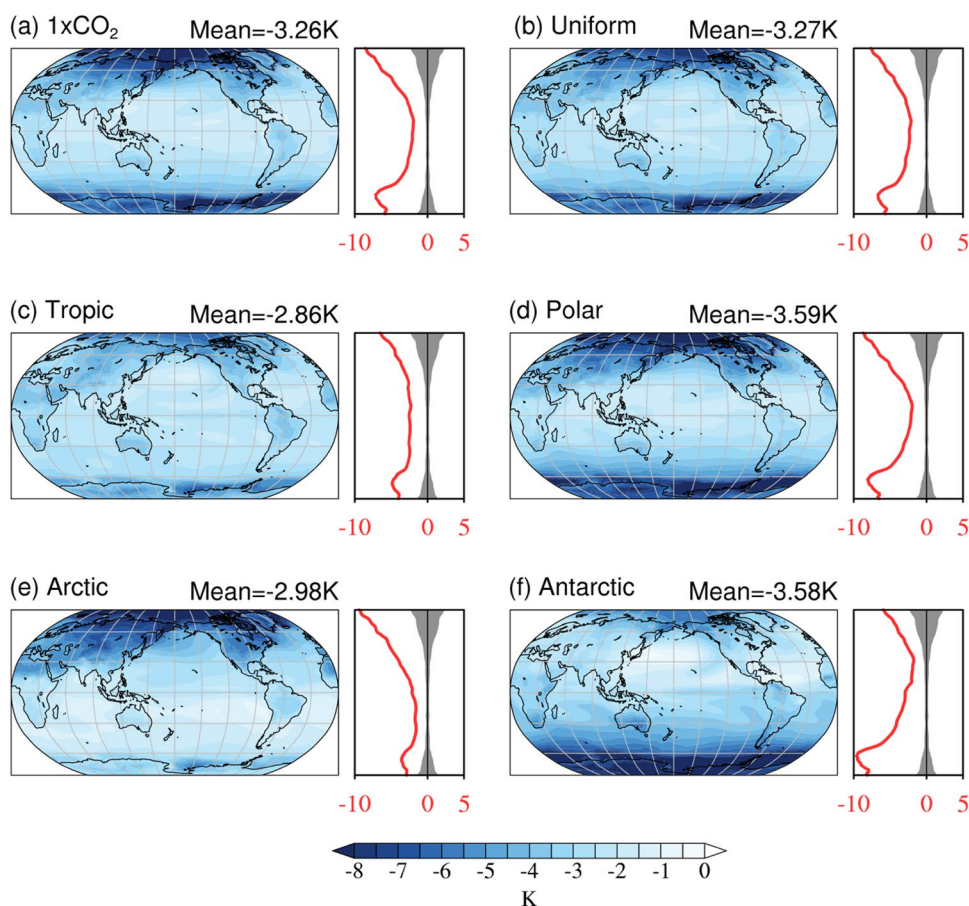


Fig. 3 **a** Interhemispheric ERF difference (IHERF, in units of Wm^{-2}) vs interhemispheric AOD difference (Δ IHAOD) and **b** interhemispheric temperature difference (Δ IHT, in unit of K) vs IHERF. The dashed line is the best linear fit, and the regression equation is shown in each panel. Slopes of regression lines, defined as the **a** IHERF per 0.1 Δ IHAOD and **b** Δ IHT difference per unit Δ IHERF are shown in the corresponding panels. The uncertainty in the slope of regression line is estimated as one-half of the difference between maximum and minimum slopes (Michael 2003)

A recent modeling study Stuecker et al. (2018) uses both the slab ocean and fully coupled configurations of the NCAR CESM model and finds that CO_2 forcing in the polar regions results in much larger climate sensitivity than in the tropics, which is in agreement with this study. In fully coupled climate model simulations, it has been shown that the ocean heat uptake efficacy has a strong dependence on geographic location (Rose and Rayborn 2016), and a sensitivity analysis of global surface temperature to ocean heat convergence forcing shows that the polar forcing causes greater global

Fig. 4 The spatial pattern of changes in annual surface temperature (K) in the $1 \times \text{CO}_2$ simulation and five geoengineering experiments relative to the $2 \times \text{CO}_2$ simulation. The changes are significant everywhere at the 95% confidence level estimated by a student's t test for 60 annual means corresponding to the last 60 years of the 100-year simulations. The changes in global mean surface temperature are shown in the top right of the panels. The subpanel on the right of each panel shows the zonal mean changes and the gray shading represents ± 2 standard deviation estimated from the $1 \times \text{CO}_2$ simulation



cooling/warming efficacy compared to the tropics (Liu et al. 2018).

The cooling produced by SAG reduces global mean precipitation (Fig. 5; Bala et al. 2008; Tilmes et al. 2013; Modak and Bala 2014; Nalam et al. 2018; Krishnamohan et al. 2019). We calculate the changes in precipitation in the five SAG experiments relative to the $2 \times \text{CO}_2$ simulation. In agreement with previous climate modelling studies (Nalam et al. 2018; Krishnamohan et al. 2019; Zhao et al. 2021), we simulate a reduction in global mean precipitation by $5.4 \pm 0.0\%$ when the concentration of CO_2 in the atmosphere is reduced by half (Fig. 5). The Uniform, Tropic and Polar cases simulate a reduction in global mean precipitation of $7.9 \pm 0.0\%$, $7.6 \pm 0.0\%$ and $8.1 \pm 0.1\%$, respectively (Fig. 5). The spatial pattern of precipitation change in the $1 \times \text{CO}_2$ case is similar to the cases with AOD values symmetric about the equator (Uniform, Tropic and Polar cases), albeit with different magnitudes. Similarity in precipitation patterns is likely associated with the similarity in the pattern of temperature change (Fig. 4) and a potential manifestation of the mode behaviour in the system (Lu et al. 2021). The largest decline in precipitation is simulated for the Antarctic case ($8.8 \pm 0.1\%$) and the smallest decline is simulated in the Arctic case ($7.3 \pm 0.0\%$, Fig. 5). The difference in

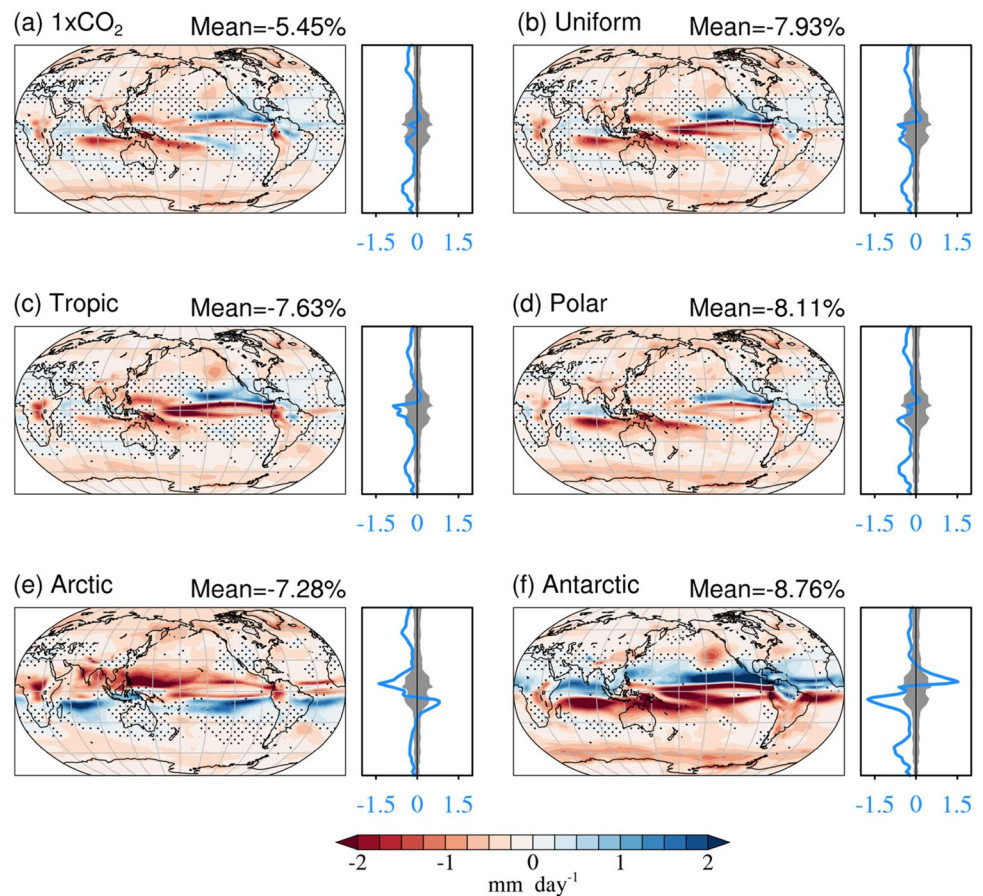
precipitation changes can be associated with the difference in global mean surface cooling and the shifts in the location of ITCZ in response to the interhemispheric temperature difference (Zhao et al. 2021). An increase in the tropical precipitation in the SH and a decrease in the NH is simulated in the Arctic case. In the Antarctic case this pattern reverses where an increase in precipitation is simulated in the NH (Fig. 5).

Several previous studies Donohoe et al. (2013), Devaraju et al. (2015), Nalam et al. (2018), Zhao et al. (2021) and Krishnamohan and Bala (2022) have shown a link between changes in the position of ITCZ and interhemispheric temperature difference. The associated changes in atmospheric heat transfer at the equator and the changes in tropical monsoon precipitation are also shown. In this study, we focus on the interhemispheric AOD difference, and quantify its effects on the location of ITCZ and, thereby, monsoon precipitation at global and regional scales.

3.3 Tropical monsoon responses

We examine changes in tropical monsoon precipitation in response to SAG and the sensitivity to the meridional distribution of stratospheric sulfate aerosols. Following

Fig. 5 The spatial pattern of changes in precipitation in the $1\times\text{CO}_2$ simulation and in the five geoengineering experiments relative to the $2\times\text{CO}_2$ simulation. The percentage change in global mean precipitation is shown in the top right of each panel. Stippled areas represent regions where changes are not significant at the 95% confidence level estimated by a student's *t* test for 60 annual means corresponding to the last 60 years of the 100-year simulations. The subpanel on the right of each panel shows the zonal mean changes and the gray shading represents ± 2 standard deviation estimated from the $1\times\text{CO}_2$ simulation



the criteria discussed in Wang and Ding (2006), we define the tropical summer monsoon regions as the areas where the local summer minus winter precipitation rate exceeds 180 mm/year, and the local summer precipitation exceeds 35% of annual precipitation. For the NH, the summer season extends from June to August and the monsoon precipitation domain consists of three regions: South Asian monsoon (SAs), North African monsoon (NAf) and North American monsoon (NA). For the SH, the summer season extends from December to February and the monsoon precipitation domain consists of three regions: Australian monsoon (AUS), South African monsoon (SAf) and South American monsoon (SA).

Figure S2 shows the tropical monsoon regions based on the precipitation from the slab ocean simulation ($2\times\text{CO}_2$). The tropical monsoon regions defined here (Fig. S2) are similar to those identified in Krishnamohan and Bala (2022). Since our study investigates only the tropical monsoon regions that are influenced by the ITCZ movement, we do not consider the East-Asian monsoon as it is a subtropical monsoon system (Wang and Lin 2002). Also, in this analysis, we account for the precipitation changes only over the land monsoon regions shown in Fig. S2. Mean precipitation in the tropical monsoon regions can be influenced

by a change in the global mean surface temperature (Chou et al. 2013) and a change in the interhemispheric temperature difference (Chiang and Friedman 2012; Friedman et al. 2013). Accordingly, previous modeling studies also show that an increased summer insolation over NH can enhance the NH summer monsoon (Zhao and Harrison 2012; Jiang et al. 2015) and a decline in insolation can lead to reduction in precipitation (Devaraju et al. 2015).

The NH monsoon is a significant component of the Earth's hydrological cycle as it provides water resources for the livelihood of 60% of the world's population (Sun et al. 2019). Future climate projections indicate that global warming would lead to an overall enhancement in the global monsoon precipitation by the end of the twenty-first century (Hsu et al. 2013) with a larger increase in the NH (Wang et al. 2020), including the Indian region (Katzenberger et al. 2021). A multi-model study by Wang et al. (2020) show that the total land monsoon precipitation is likely to increase in the NH (2.8% per 1°C of global warming), and the increase is likely to be smaller in the Southern Hemisphere (SH).

In our simulations, we find that the NH summer monsoon index (NHMI; summer monsoon precipitation over NH monsoon regions) decreases in all SAG experiments except in the Antarctic case relative to the $2\times\text{CO}_2$

simulation (Fig. 6a). The Uniform, Tropic, Polar, Arctic and Antarctic cases show a change in NHMI of $-3.7 \pm 0.7\%$, $-1.9 \pm 0.7\%$, $-6.6 \pm 0.7\%$, $-16.5 \pm 0.6\%$ and $+9.2 \pm 0.8\%$, respectively (Fig. 6a), indicating that the Arctic and Antarctic cases simulate the largest decline and an enhancement in NHMI, respectively. The tropical SH summer monsoon index (SHMI; summer monsoon precipitation over SH monsoon regions) reduces in all the SAG experiments (Fig. 6b) with least reduction in the Arctic case ($-4.0 \pm 0.7\%$). The largest decline in SHMI is simulated in the Antarctic case ($-16.9 \pm 0.5\%$, Fig. 6b). The reduction in monsoon precipitation can be associated with the decrease in global mean surface temperature in the SAG experiments relative to the $2 \times \text{CO}_2$ case. Besides the global mean surface temperature, the latitudinal position of ITCZ is one of the primary factors controlling tropical monsoon precipitation. Hence, we analyze the response of ITCZ to the interhemispheric AOD difference in SAG experiments. Similar to previous studies (Donohoe et al. 2013; Devaraju et al. 2015; Nalam et al. 2018), the mean position of ITCZ is identified using the precipitation centroid (P_{cent}), the median latitude of zonal mean area-weighted precipitation between 20°S and 20°N after interpolating the precipitation data to a 0.01° grid. We estimate a sensitivity of $-1.8^\circ \pm 0.0^\circ$ meridional shift in global mean ITCZ per 0.1 interhemispheric AOD difference (Fig. 7a). A sensitivity of $0.9^\circ \pm 0.0^\circ$ and $1.5^\circ \pm 0.1^\circ$ meridional shift is also estimated per unit (Wm^{-2}) interhemispheric

differences in ERF and interhemispheric temperature ($^\circ\text{C}$) difference, respectively (Fig. 7b, c).

In the Arctic case, the larger AOD values in the NH (Fig. 2) cause more cooling in the NH than the SH (Fig. 4) which leads to a larger interhemispheric temperature contrast (Fig. 3). As a response to the interhemispheric temperature contrast in Arctic case, the ITCZ shifts southward by about 2.5° latitudes towards the warmer SH (Fig. 7). Thus, due to the cooling in NH and associated shift in ITCZ, a decrease of more than 15% in NHMI is simulated in the Arctic case (Fig. 6a). In the Antarctic case, the interhemispheric radiative forcing asymmetries associated with larger AOD values in the SH result in an interhemispheric temperature difference (Fig. 3), which causes the ITCZ to shift to the relatively warmer NH (Fig. 7) and thereby enhancing the NH monsoon precipitation (NHMI) by $\sim 9\%$ (Fig. 6a). Therefore, the NHMI changes under the Arctic and Antarctic cases are primarily associated with interhemispheric AOD differences (Fig. 8). The changes in NHMI have strong negative correlation with the interhemispheric AOD difference (mean AOD in the NH minus SH) with a linear regression coefficient of $-6.9 \pm 0.4\%$ per 0.1 interhemispheric AOD difference (Fig. 8, Table S1). In contrast, the changes in SH summer monsoon precipitation (SHMI) and interhemispheric AOD differences show a positive correlation, with an increase in the monsoon precipitation by about $3.4 \pm 0.3\%$ per 0.1 AOD interhemispheric difference (Figure S3a, Table S1).

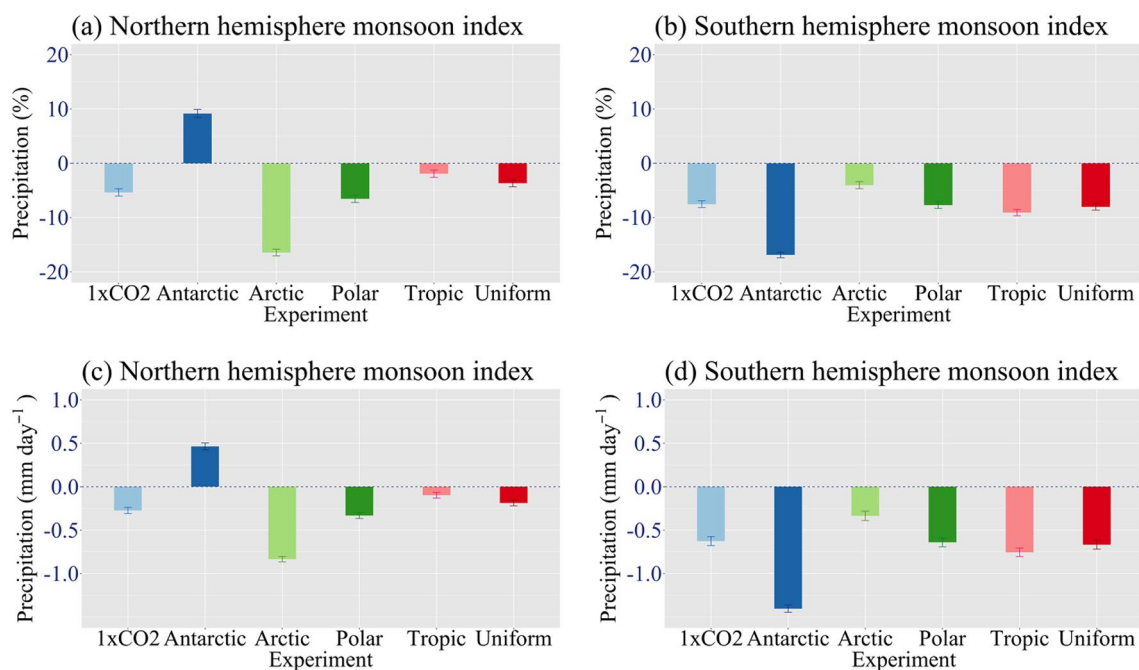


Fig. 6 Percentage changes in the **a** northern hemisphere and **b** southern hemisphere monsoon precipitation index in the $1 \times \text{CO}_2$ simulation and in the five geoengineering experiments relative to the $2 \times \text{CO}_2$ simulation. Absolute changes in the **c** north-

ern hemisphere and **d** southern hemisphere monsoon precipitation index (mm/day). Error bars represent standard error (standard deviation/ $\sqrt{\text{sample size}}$) calculated from the last 60 years of 100-year slab-ocean simulations

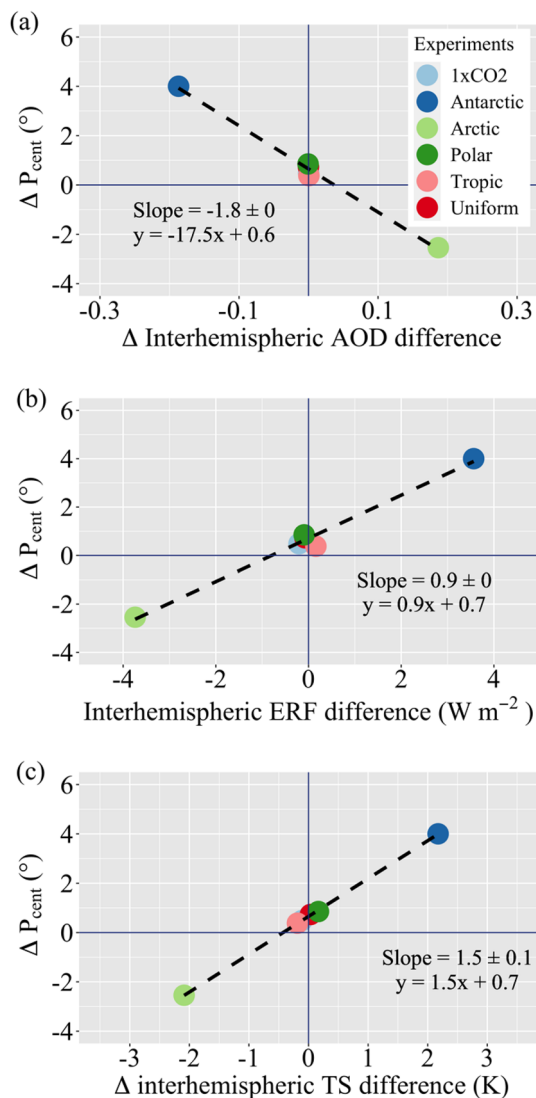


Fig. 7 Changes in tropical precipitation centroid (P_{cent}) vs **a** change in interhemispheric AOD difference (ΔIHAOD), **b** interhemispheric ERF difference (ΔHERF , in units of W m^{-2}), and **c** change in interhemispheric temperature difference (ΔIHT , in unit of K). The dashed line is the best linear fit, and the regression equation is shown in each panel. Slopes of regression lines, defined as the **a** change in P_{cent} per 0.1 ΔIHAOD , **b** per unit ΔHERF , and **c** per unit ΔIHT are shown in the corresponding panels. The uncertainty in the slope of regression line is estimated as one-half of the difference between maximum and minimum slopes (Michael 2003)

The sensitivity analysis also indicates that the regression lines do not pass through the origin and y-intercepts give an estimate of 4.1% (Fig. 8a) and 8.9% (Figure S3a) reduction in the NHMI and SHMI, respectively, indicating that the tropical monsoon precipitation decreases even in the Uniform, Tropic and Polar cases with no interhemispheric AOD difference (Fig. 8a, Figure S3a). The decrease in monsoon precipitation in these cases is due to an increase in global mean AOD. A slight northward shift in the position of ITCZ

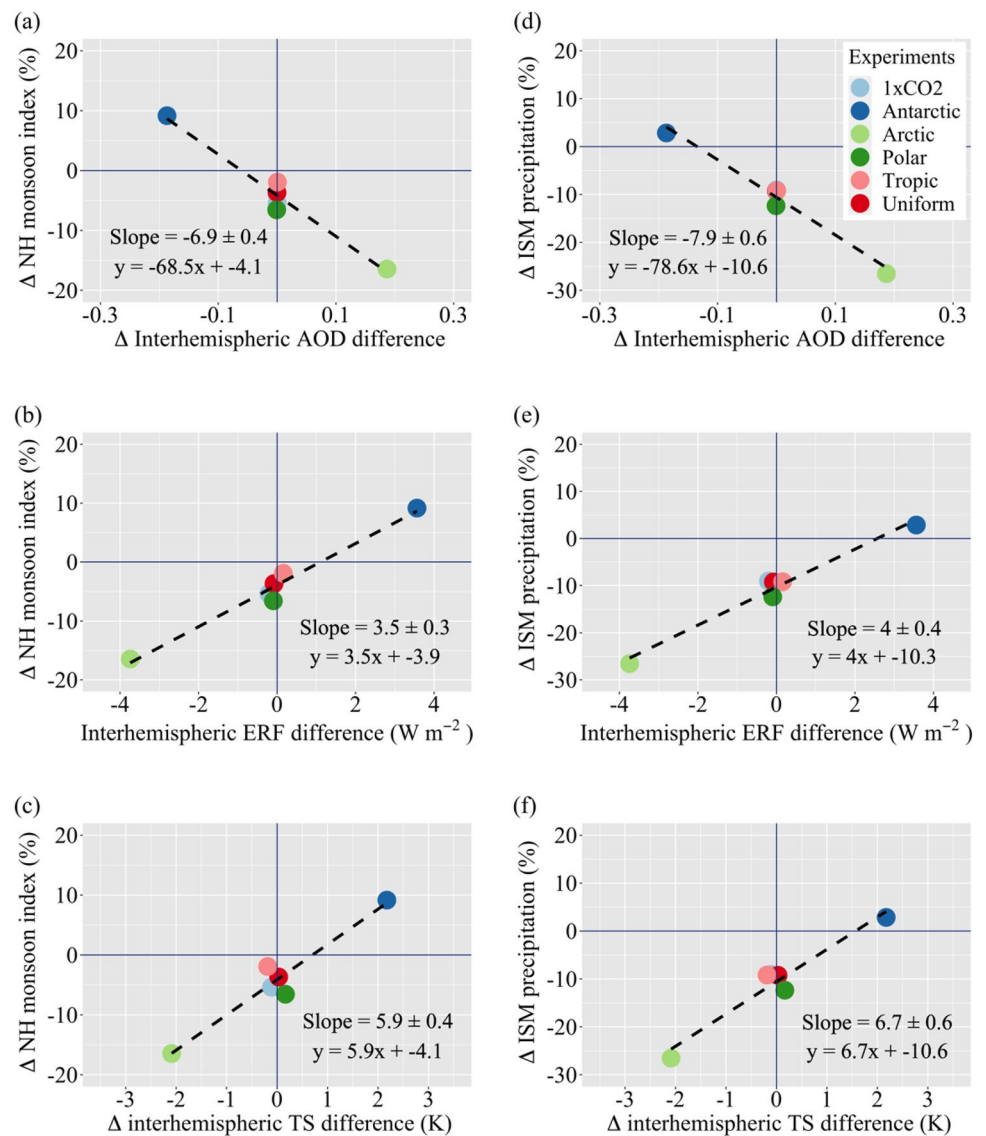
in the cases of no interhemispheric AOD difference (Fig. 7) results in a smaller decrease in the NHMI (Fig. 8a) but a relatively larger decrease in the SHMI (Figure S3a) in these cases. Regardless of the location of the forcing, such a tendency for the ITCZ to shift northward in slab-ocean simulations may arise from the asymmetry in land distribution between the hemispheres and the intrinsic nonlinearity of the climate system (Harrop et al. 2018). Our results demonstrate that the monsoon precipitation changes in the two hemispheres are contributed by two factors, globally mean AOD and interhemispheric AOD difference.

We also estimate the sensitivity of NHMI and SHMI in terms of interhemispheric differences in ERF and interhemispheric temperature differences. The slopes in Fig. 8b and S3b indicate a NHMI sensitivity of a $3.5 \pm 0.3\%$ increase (Table S1) and a $1.8 \pm 0.1\%$ (Table S1) decrease in SHMI per unit interhemispheric difference in ERF (per W m^{-2}). The slopes in Figs. 8c and S3c indicate a sensitivity of $5.9 \pm 0.4\%$ increase in NHMI (Table S1) and $3.0 \pm 0.2\%$ decrease in SHMI (Table S1) per unit interhemispheric temperature differences (1 K). For the tropical monsoon index (TMI, sum of the NHMI and SHMI), the changes in NHMI and SHMI nearly offset each other (Figure S3d; no significant slope of regression line). The sensitivity analysis of TMI in terms of interhemispheric differences in AOD, ERF and temperature indicate no significant slope in the regression lines and the y-intercepts of $\sim 7\%$ decrease in TMI is due to an increase in the global mean AOD.

Analysis of individual monsoon region indicates that all the tropical monsoon regions except the North American monsoon region show a decline in summer monsoon precipitation (Fig. S4) in response to the solar dimming by SAG. The Antarctic case with the highest AOD values in the SH (Fig. 2) leads to a northward shift of ITCZ to the warmer NH (Fig. 7a) and enhances (declines) the monsoon precipitation over NH (SH) monsoon regions. The SH monsoon precipitation declines in all the SAG experiments and the least reduction is simulated in the Arctic case (Fig. 6b). In general, the summer monsoon precipitation decreases in the hemisphere with larger sulfate AOD values and increases in the opposite hemisphere.

A recent study by Krishnamohan and Bala (2022) estimated the impact of varying the latitudinal position of aerosol injection on the global monsoon precipitation and found that the hemispheric mean summer monsoon precipitation declines in the hemisphere where aerosols are injected and enhances in the opposite hemisphere. Their study investigated the transient responses of a coupled ocean–atmosphere model with continuously increasing concentrations of greenhouse gases. In contrast, we have used slab-ocean simulations to study equilibrium climate change. Therefore, our estimates of monsoon precipitation changes per 0.1 interhemispheric AOD difference in our equilibrium slab-ocean

Fig. 8 Changes in northern hemisphere monsoon precipitation index (left panels) vs **a** changes in Interhemispheric AOD difference (Δ IHAOD), **b** Interhemispheric ERF difference (IHERF, in units of W m^{-2}), and **c** changes in interhemispheric temperature difference (Δ IHT, in unit of K), and corresponding changes in Indian summer monsoon (ISM) precipitation (right panels) vs **d** Δ IHAOD, **e** IHERF and **f** Δ IHT. The dashed line is the best linear fit, and the regression equation is shown in each panel. Slopes, defined as the **a**, **d** change in monsoon indices per 0.1 Δ IHAOD, **b**, **e** per unit Δ IHERF, and **c**, **f** per unit Δ IHT are shown in the corresponding panels. The uncertainty in the slope of regression line is estimated as one-half of the difference between maximum and minimum slopes (Michael 2003)



simulations are larger when compared to the fully coupled transient simulations used in Krishnamohan and Bala (2022). The lack of deep ocean dynamics in our slab ocean simulations is likely the source for difference in monsoon precipitation sensitivity between our study and Krishnamohan and Bala (2022) which uses fully coupled simulations. Further, in the real world, anthropogenic aerosols (Smith et al. 2011) affect the cloud properties through aerosol–cloud interactions in the troposphere (Haywood and Ramaswamy 1998). However, our geoengineering simulations are forced with highly idealized distributions of reflective sulfate aerosols injected only into the stratosphere.

The sulfate AOD patterns in our study differ from Krishnamohan and Bala (2022). For instance, in their study, sulfate injection at 30° S (30° N) increases sulfate AOD only in the southern (northern) hemisphere. In our

study, in the Arctic and Antarctic cases with the aerosol distribution asymmetric about the equator, the sulfate AOD varies gradually from one pole to another. Moreover, in all our SAG experiments, AOD increases in all regions (Fig. 2). In our simulations, the hemispherically asymmetric distribution of sulfate aerosols in the Arctic and Antarctic cases are created by making use of the linear combinations of Legendre polynomial of order zero and one. The parabolic distributions in the Tropic and Polar cases are created by the linear combinations of Legendre polynomial of order zero and two. More simulations using such multiple hemispherically asymmetric patterns of aerosols would help to test the robustness of our results. Simulations using multiple models would be useful to quantify the uncertainties.

3.4 Response of the Indian summer monsoon to SAG

The Indian summer monsoon season, which lasts from June to September, contributes about 80% to the annual precipitation of India and impacts the lives of more than one billion people (Mooley and Parthasarathy 1984; Turner and Annamalai 2012). The Indian summer monsoon is one of the significant atmosphere–ocean coupled climate systems in the tropics, and it exhibits large variability at interannual and intraseasonal timescales (Goswami and Mohan 2001; Goswami and Chakravorty 2017).

In response to a doubling of CO_2 in the atmosphere ($2 \times \text{CO}_2$ simulation), the mean surface temperature in India during the summer monsoon season increases by about 2.2 K (Fig. S5a), and the summer monsoon precipitation in India increases by about 9% (Fig. 9a). Aerosol-induced solar dimming can reduce evaporation from the north Indian Ocean and the Indian sub-continent, which is the primary source for water vapour for the Indian monsoon (Ramanathan et al. 2005). Recent modeling studies indicate that an increase in stratospheric sulphate aerosols can reduce the precipitation in India (Sherman et al. 2020; Krishnamohan and Bala 2022). We quantify the monsoon precipitation sensitivity in terms of interhemispheric AOD difference (Fig. 8d). We find that the Indian monsoon precipitation decreases by $7.9 \pm 0.6\%$ per 0.1 interhemispheric AOD difference (Fig. 8d, Table S1). The y-intercept of 10.6% reduction in the monsoon precipitation is caused by the global mean increase in AOD (Fig. 8d). The slopes in Fig. 8e and f indicate a precipitation sensitivity of $4.0 \pm 0.4\%$ and $6.7 \pm 0.6\%$ (Table S1) increase in terms of unit interhemispheric differences in ERF (per Wm^{-2}) and surface temperature change (per K).

In the Uniform case, the surface temperature over India during summer monsoon season decreases by 2.4 K relative to the $2 \times \text{CO}_2$ simulation, which nearly offsets the mean summer warming from a doubling of CO_2 concentration (Fig. S5a). In response to the cooling, the Indian summer monsoon precipitation decreases by about 9.3% in the Uniform simulation (Fig. 9b) relative to the $2 \times \text{CO}_2$ simulation. In the Tropic, Polar, Arctic and Antarctic cases, surface cooling over India ranges from -1.6 to -3.2 K (Fig. S5). The Antarctic case simulates the maximum cooling (~ 3 K) in the Indian region during the monsoon season (Fig. S5), because the northward shift in the ITCZ location is associated with an increase in cloud cover over the Indian region (Fig. S6), reducing shortwave radiation reaching the surface (Fig. S7) and thus leading to larger surface cooling.

Figure 9 shows the changes in Indian summer monsoon precipitation in each experiment relative to the $2 \times \text{CO}_2$ case. The Indian summer monsoon precipitation decreases in the $1 \times \text{CO}_2$ case relative to the $2 \times \text{CO}_2$ simulation (Fig. 9a)

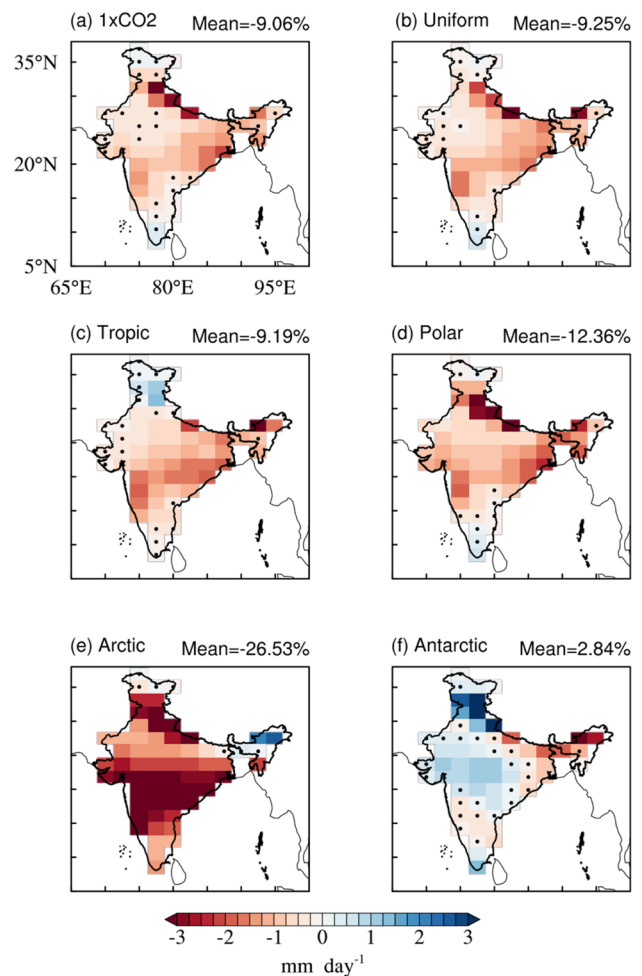


Fig. 9 The changes in Indian summer monsoon precipitation (June to September) in the $1 \times \text{CO}_2$ simulation and in the stratospheric aerosol geoengineering simulations relative to the $2 \times \text{CO}_2$ simulation. Stippled areas represent regions where changes are not significant at the 95% confidence level estimated by a student's *t* test for 60 seasonal means corresponding to the last 60 years of the 100-year simulations. The mean changes over India are shown at the top right of each panel

because of global mean cooling. According to the criteria adopted by Indian Meteorological Department (IMD-Met Glossary 2023), a year with more than 10% deficit in the monsoon precipitation from long term climatological mean and when the spatial coverage of the deficiency is more than 20% of the country is considered as a drought year. 10% is approximately the standard deviation of Indian summer monsoon precipitation (Gadgil 2018; Roose et al. 2019). Relative to the $2 \times \text{CO}_2$ simulation, the change in the Indian summer monsoon precipitation in the Uniform, Tropic, Polar, Arctic, and Antarctic cases is -9.3% , -9.2% , -12.4% , -26.5% and $+2.8\%$, respectively (Fig. 9), indicating that the monsoon precipitation decreases in all geoengineering simulations except the Antarctic case. In the Antarctic case, the monsoon precipitation increases over the

most parts of India except northeast India. A relatively larger increase in AOD in NH in the Arctic case leads to enhanced cooling in NH and causes a southward shift in the ITCZ in the Indian Ocean. The meridional change in the position of ITCZ is crucial for the Indian summer monsoon precipitation (Fleitmann et al. 2007; Hari et al. 2020). In the Arctic case, a southward shift of ITCZ to the relatively warmer SH reduces the precipitation over most parts of India (Fig. 9e). The simulated reduction in the Indian summer monsoon precipitation is more than 26% in the Arctic case (Fig. 9e), which is the largest reduction over India in our geoengineering simulations. Therefore, frequent droughts are likely over India if stratospheric aerosols are used to offset global warming and maximized in the Arctic region.

4 Summary and conclusions

In this study, we have used the Community Earth System Model (CESM) to investigate the impact of different meridional distributions of sulfate aerosol (Fig. 1a) in the stratosphere (37 hPa) on the tropical monsoon and the Indian summer monsoon precipitation. The aerosol-induced cooling in our Stratospheric Aerosol Geoengineering (SAG) simulations partially offsets the warming from a doubling of CO₂ concentration except in the Antarctic and Polar simulations where global mean warming is overcompensated (Figs. 4). In response to SAG, a decline in global mean precipitation is simulated in the geoengineering simulations, with a maximum reduction of up to about 8.8% in the Antarctic case (Fig. 5). The NH summer (June–August) monsoon precipitation decreases in all cases except in the Antarctic case (Fig. 6). The asymmetric sulphate aerosol distribution about the equator leads to changes in interhemispheric AOD differences, which result in more negative radiative forcing in one hemisphere relative to the other (Fig. 3a). In our simulations, the interhemispheric AOD and ERF differences are negatively correlated with a linear regression coefficient of $\sim 2 \text{ Wm}^{-2}$ per 0.1 AOD difference.

The interhemispheric ERF difference leads to interhemispheric surface temperature difference ($\sim 0.6 \text{ K}$ increase per Wm^{-2} , Fig. 3b). This interhemispheric temperature contrast is associated with a shift in the location of ITCZ into the warmer hemisphere (Fig. 7). In our simulations, we find that the interhemispheric AOD difference is correlated with ITCZ shift with a linear regression coefficient of $-1.8 \pm 0.0^\circ$ per 0.1 interhemispheric AOD difference (Fig. 7a). The asymmetric AOD changes about the equator and resulting ITCZ shifts in the SAG experiments alter the spatial distribution precipitation, with a reduction in the NH summer monsoon precipitation in the Arctic case (Fig. 8). The AOD increase in the SH in the Antarctic case enhances the NH monsoon precipitation. We estimate a sensitivity of

$6.9 \pm 0.4\%$ reduction in NH summer monsoon precipitation per 0.1 interhemispheric AOD difference (Fig. 8, Table S1). In cases with hemispherically symmetrical aerosol loading (Uniform, Tropic and Polar cases), the slight decline in NH monsoon precipitation (Figs. 6a, 8) is due to an increase in the global mean AOD. Thus, we find that both global-mean surface cooling due to global-mean AOD increases and the ITCZ shift due to interhemispheric AOD difference cause changes in tropical monsoon precipitation. We also estimate the sensitivity of SH summer monsoon precipitation in terms of interhemispheric differences in AOD, ERF and temperature. The sensitivity of the SH summer monsoon precipitation is $-3.0 \pm 0.2\%$ per unit interhemispheric temperature ($^\circ\text{C}$) difference, $-1.8 \pm 0.1\%$ per unit (Wm^{-2}) interhemispheric differences in ERF and $3.4 \pm 0.3\%$ per 0.1 interhemispheric AOD difference (Table S1). Our results are consistent with a recent assessment of declining trend in the South Asian and North African monsoon precipitation during the second half of the twentieth century due to the radiative effects of NH anthropogenic aerosols (IPCC 2021b SPM, Douville et al. 2021).

The Indian summer monsoon is reduced in cases with AOD changes that are symmetric about the equator (Uniform, Tropic and Polar cases) due to the aerosol induced surface cooling. However, the maximum reduction (of 26.5%) in Indian monsoon precipitation is simulated in the Arctic case (Fig. 9). The Arctic case with the largest increase in AOD values in the NH creates more cooling in the NH than the SH. Larger cooling in NH leads to a southward ITCZ shift to the relatively warmer SH, adversely affecting Indian summer monsoon precipitation. Therefore, in the Arctic case, the Indian monsoon precipitation decreases due to a global-mean cooling of $\sim 3 \text{ K}$ in association with an increased global mean AOD and a southward shift in ITCZ associated with an increase in interhemispheric AOD difference. In the Antarctic case, the northward shift of ITCZ leads to an enhancement of the Indian summer monsoon by $\sim 3\%$. The sensitivity of the Indian summer monsoon precipitation is estimated as $6.7 \pm 0.6\%$ per unit ($^\circ\text{C}$) interhemispheric temperature difference, $4.0 \pm 0.4\%$ per unit (Wm^{-2}) interhemispheric differences in ERF and $-7.9 \pm 0.6\%$ per 0.1 interhemispheric AOD difference (Table S1). The sensitivity of tropical monsoon precipitation indices is summarized in Fig. 10 and Table S1.

There are several limitations to our study. First, we have performed equilibrium simulations using a slab-ocean model and hence our simulations do not include the transient effects of climate change and deep ocean dynamics. As ocean heat transport is prescribed in slab ocean simulations, the atmospheric heat transport across the equator and the associated ITCZ shifts and precipitation changes in the tropical monsoon regions are likely overestimated in our simulations. This is evident when our results are compared

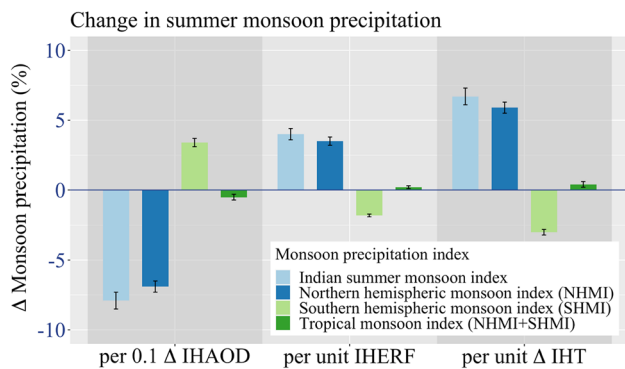


Fig. 10 Sensitivity of tropical monsoon precipitation indices for the interhemispheric AOD difference (Δ IHAOD), interhemispheric effective radiative forcing difference (IHERF), and changes in interhemispheric temperature difference (Δ IHT). The change (Δ) in the SAG-cases is relative to the $2\times\text{CO}_2$ climate simulation in the last 60-years of 100-year slab-ocean simulations. The sensitivity is estimated from the linear regression analysis and the error bars represent uncertainty as one-half of the difference between the maximum and minimum slopes of the regression line (Michael 2003)

to Krishnamohan and Bala (2022) which uses data from transient coupled simulations with full ocean dynamics. Analysis using transient simulations from coupled climate models driven by idealized forcing like in our study merits further studies.

Second, we have prescribed sulfate aerosol concentrations in the stratosphere with highly idealized distributions with no seasonal changes. Thus, our modeling framework lacks the explicit representation of complex aerosol processes such as aerosol microphysics, aerosol chemistry, transport and sedimentation. The time and location where aerosol injected into the stratosphere can impact the spatial distribution of aerosols and AOD (MacMartin et al. 2017; Vioni et al. 2019, 2020). However, the use of a simpler modelling framework with idealized aerosol distributions help us isolate and study the sensitivity to individual factors such as the pattern of aerosol distribution that are challenging in more complex model configurations.

Third, as the aerosols are prescribed in the stratosphere in our simulations, direct aerosol–cloud interactions not simulated and hence the sensitivity to AOD changes estimated in this study are relevant to only stratospheric sulfate aerosols and not relevant to tropospheric aerosols. As aerosol–cloud interaction in the troposphere leads to more negative radiative forcing (Forster et al. 2021), it is likely that changes in global mean AOD and interhemispheric AOD differences due to tropospheric aerosols could lead to larger sensitivity of tropical monsoon precipitation to AOD changes than our estimates. Further, we have assessed the sensitivity of tropical monsoon precipitation only to sulfate aerosols which are highly reflective. The sensitivity of ITCZ shifts and monsoon precipitation change would be different for aerosols

with different optical properties such as black carbon (Wang 2004; Modak and Bala 2014; Krishnamohan et al. 2021).

Our estimates of the sensitivity of the ITCZ shift, and changes in hemispheric and Indian monsoon precipitation per unit changes in interhemispheric AOD differences and interhemispheric radiative forcing are based only on the Arctic and Antarctic experiments. To assess the robustness of these sensitivities, we added two more points to the regressions as shown in Figs. S8, S9 and S10. The additional points represent simulations which are similar to the Arctic and Antarctic simulations with same amount of sulfate aerosol, but the meridional distribution is linear in latitudes rather than sine of latitudes. Robustness of our estimates is indicated as the two new points fall on the same line. Nevertheless, we plan to perform multiple simulations with different interhemispheric AOD differences to improve our estimates of the sensitivities in a future study. Finally, our results are based on a single model and future work based on multi-model simulations will be required to assess the uncertainty and robustness of the results from this study.

Supplementary Information The online version contains supplementary material available at <https://doi.org/10.1007/s00382-023-06799-3>.

Acknowledgements This work was supported by the National Supercomputer Mission (Reference number: DST/NSM/R&D_HPC Applications/2021/03.09) under the department of science and technology (DST), Government of India. We would like to acknowledge the high-performance computing support from the Supercomputer Education and Research Centre (SERC) team, Indian Institute of Science, Bangalore. We are thankful to the Earth Commission which facilitated discussions on the effects of aerosol loading on the tropical monsoon precipitation.

Author contributions SR, GB, LC and KC contributed to the design of experiments. SR performed the simulations. SR, GB, and KSK performed the analysis and wrote the manuscript. LC and KC reviewed and edited the manuscript.

Funding This work was funded by the Department of Science and Technology (DST), Government of India (DST/NSM/R&D_HPC_Applications/2021/03.09 and DST/CCP/NMSKCC/MRDP/210/2022(G)) and the Degrees Modeling Fund (DMF) from the Degrees Initiative.

Declarations

Conflict of interest Authors have no competing financial and/or non-financial interests.

Data availability The datasets and codes used for the current study are available from the corresponding author on reasonable request.

Open Access This article is licensed under a Creative Commons Attribution 4.0 International License, which permits use, sharing, adaptation, distribution and reproduction in any medium or format, as long as you give appropriate credit to the original author(s) and the source, provide a link to the Creative Commons licence, and indicate if changes were made. The images or other third party material in this article are included in the article's Creative Commons licence, unless indicated

otherwise in a credit line to the material. If material is not included in the article's Creative Commons licence and your intended use is not permitted by statutory regulation or exceeds the permitted use, you will need to obtain permission directly from the copyright holder. To view a copy of this licence, visit <http://creativecommons.org/licenses/by/4.0/>.

References

- Aldy JE, Felgenhauer T, Pizer WA, Tavoni M, Belaia M, Borsuk ME, Wiener JB (2021) Social science research to inform solar geoengineering. *Science* 374(6569):815–818. <https://doi.org/10.1126/science.abj6517>
- Ammann CM, Meehl GA, Washington WM, Zender CS (2003) A monthly and latitudinally varying volcanic forcing dataset in simulations of 20th century climate. *Geophys Res Lett* 30(12):1–4. <https://doi.org/10.1029/2003GL01687>
- Bailey DA, Holland M, Hunke EC et al (2010) Community Ice Code (CICE) User's Guide Version 4.0. Documentation 0–22
- Bala G, Duffy PB, Taylor KE (2008) Impact of geoengineering schemes on the global hydrological cycle. *Proc Natl Acad Sci USA* 105:7664–7669. <https://doi.org/10.1073/pnas.0711648105>
- Ban-Weiss GA, Caldeira K (2010) Geoengineering as an optimization problem. *Environ Res Lett* 5:1–2. <https://doi.org/10.1088/1748-9326/5/3/034009>
- Berry G, Reeder MJ (2014) Objective identification of the intertropical convergence Zone: climatology and trends from the ERA-Interim. *J Clim* 27(5):1894–1909. <https://doi.org/10.1175/JCLI-D-13-00339.1>
- Budyko MI (1977) Climatic changes. American Geophysical Union, Washington DC
- Caldeira K, Bala G, Cao L (2013) The science of geoengineering. *Annu Rev Earth Planet Sci* 41:231–256. <https://doi.org/10.1146/annurev-earth-042711-105548>
- Cheng W, MacMartin DG, Kravitz B, Visionsi D, Bednarz EM, Xu Y, Deng X (2022) Changes in Hadley circulation and intertropical convergence zone under strategic stratospheric aerosol geoengineering. *NPJ Clim Atmos Sci*. <https://doi.org/10.1038/s41612-022-00254-6>
- Chiang JC, Friedman AR (2012) Extratropical cooling, interhemispheric thermal gradients, and tropical climate change. *Annu Rev Earth Planet Sci* 40:383–412. <https://doi.org/10.1146/annurev-earth-042711-105545>
- Chou C, Chiang JC, Lan CW, Chung CH, Liao YC, Lee CJ (2013) Increase in the range between wet and dry season precipitation. *Nat Geosci* 6(4):263–267. <https://doi.org/10.1038/ngeo1744>
- Crutzen PJ (2006) Albedo enhancement by stratospheric sulfur injections: a contribution to resolve a policy dilemma? *Clim Change* 77:211–220. <https://doi.org/10.1007/s10584-006-9101-y>
- Devaraju N, Bala G, Modak A (2015) Effects of large-scale deforestation on precipitation in the monsoon regions: remote versus local effects. *Proc Natl Acad Sci USA* 112:3257–3262. <https://doi.org/10.1073/pnas.1423439112>
- Donohoe A, Marshall J, Ferreira D, Mcgee D (2013) The relationship between ITCZ location and cross-equatorial atmospheric heat transport: From the seasonal cycle to the last glacial maximum. *J Clim* 26(11):3597–3618. <https://doi.org/10.1175/JCLI-D-12-00467.1>
- Douville H, Raghavan K, Renwick J, Allan RP, Arias PA, Barlow M, Cerezo-Mota R, Cherchi A, Gan TY, Gergis J, Jiang D, Khan A, Pokam W, Rosenfeld D, Tierney J, Zolina O (2021) Water cycle changes. In: Masson-Delmotte V, Zhai P, Pirani A, Connors SL, Péan C, Berger S, Caud N, Chen Y, Goldfarb L, Gomis MI, Huang M, Leitzell K, Lonnoy E, Matthews JBR, Maycock TK, Waterfield T, Yelekçi O, Yu R, Zhou B (eds) *Climate Change 2021: the physical science basis*. Contribution of Working Group I to the Sixth Assessment Report of the Intergovernmental Panel on Climate Change. Cambridge University Press, Cambridge, pp 1055–1210. <https://doi.org/10.1017/9781009157896.010>
- Duan L, Cao L, Bala G, Caldeira K (2018) Comparison of the fast and slow climate response to three radiation management geoengineering schemes. *J Geophys Res Atmos* 123(11):980–12001. <https://doi.org/10.1029/2018JD029034>
- Ferraro AJ, Highwood EJ, Charlton-Perez AJ (2011) Stratospheric heating by potential geoengineering aerosols. *Geophys Res Lett* 38:L24706. <https://doi.org/10.1029/2011GL049761>
- Ferraro AJ, Highwood EJ, Charlton-Perez AJ (2014) Weakened tropical circulation and reduced precipitation in response to geoengineering. *Environ Res Lett*. <https://doi.org/10.1088/1748-9326/9/1/014001>
- Fleitmann D, Burns SJ, Mangini A, Mudelsee M, Kramers J, Villa I, Matter A (2007) Holocene ITCZ and Indian monsoon dynamics recorded in stalagmites from Oman and Yemen (Socotra). *Quatern Sci Rev* 26(1):170–188. <https://doi.org/10.1016/j.quascirev.2006.04.012>
- Forster P, Storelvmo T, Armour K, Collins W, Dufresne J-L, Frame D, Zhang H (2021) Earth's energy budget, climate feedbacks, and climate sensitivity. In: Masson-Delmotte V et al (eds) *Climate change 2021: the physical science basis*. Contribution of working group I to the sixth assessment report of the intergovernmental panel on climate change. Cambridge University Press, Cambridge, United Kingdom and New York, NY, USA, pp 923–1054. <https://doi.org/10.1017/9781009157896.009>
- Friedman AR, Hwang YT, Chiang JC, Frierson DM (2013) Interhemispheric temperature asymmetry over the twentieth century and in future projections. *J Clim* 26(15):5419–5433. <https://doi.org/10.1175/JCLI-D-12-00525.1>
- Gadgil S (2018) The monsoon system: land–sea breeze or the ITCZ? *J Earth Syst Sci* 127:1. <https://doi.org/10.1007/s12040-017-0916-x>
- Gent PR, Danabasoglu G, Donner LJ et al (2011) The community climate system model version 4. *J Clim* 24:4973–4991. <https://doi.org/10.1175/2011JCLI4083.1>
- Goswami BN, Chakravorty S (2017) Dynamics of the Indian summer monsoon climate. *Oxford research encyclopedia of climate science*. Oxford University Press, Oxford, pp 1–36
- Goswami BN, Mohan RSA (2001) Intraseasonal oscillations and interannual variability of the Indian summer monsoon. *J Clim* 14(6):1180–1198. [https://doi.org/10.1175/1520-0442\(2001\)014<1180:IOAIVO>2.0.CO;2](https://doi.org/10.1175/1520-0442(2001)014<1180:IOAIVO>2.0.CO;2)
- Hansen J et al (1997) Radiative forcing and climate response. *J Geophys Res Atmos* 102(D6):6831–6864. <https://doi.org/10.1029/96JD03436>
- Hansen J et al (2005) Efficacy of climate forcings. *J Geophys Res Atmos* 110:D18104. <https://doi.org/10.1029/2005JD005776>
- Hari V, Villarini G, Karmakar S, Wilcox LJ, Collins M (2020) Northward propagation of the intertropical convergence zone and strengthening of Indian Summer Monsoon Rainfall. *Geophys Res Lett*. <https://doi.org/10.1029/2020GL089823>
- Harrop BE, Lu J, Liu F, Garuba OA, Ruby Leung L (2018) Sensitivity of the ITCZ location to ocean forcing via q-flux Green's function experiments. *Geophys Res Lett* 45(13):116–13123. <https://doi.org/10.1029/2018GL080772>
- Haywood JM, Ramaswamy V (1998) Global sensitivity studies of the direct radiative forcing due to anthropogenic sulfate and black carbon aerosols. *J Geophys Res Atmos* 103(D6):6043–6058. <https://doi.org/10.1029/97JD03426>
- Haywood JM, Jones A, Bellouin N, Stephenson D (2013) Asymmetric forcing from stratospheric aerosols impacts Sahelian rainfall. *Nat Clim Chang* 3(7):660–665. <https://doi.org/10.1038/nclimate1857>

- Hsu PC, Li T, Murakami H, Kitoh A (2013) Future change of the global monsoon revealed from 19 CMIP5 models. *J Geophys Res Atmos* 118(3):1247–1260. <https://doi.org/10.1002/jgrd.50145>
- IMD-Met Glossary, 1–13. <https://www.imdpune.gov.in/Reports/glossary.pdf>. Accessed 28 April 2023
- IPCC (2021a) The physical science basis. Contribution of working group I to the sixth assessment report of the intergovernmental panel on climate change. In: Masson-Delmotte V, Zhai P, Pirani A et al (eds) Climate change 2013: contribution of Working group I to the fifth assessment report of the intergovernmental panel on climate change. Cambridge University Press (In Press)
- IPCC (2021b) Summary for policymakers. In: Climate change 2021: the physical science basis. Contribution of working group I to the sixth assessment report of the intergovernmental panel on climate change. In: Masson-Delmotte V, Zhai P, Pirani A et al (eds) Cambridge University Press, Cambridge, pp 3–32. <https://doi.org/10.1017/9781009157896.001>
- Irvine P, Emanuel K, He J, Horowitz LW, Vecchi G, Keith D (2019) Halving warming with idealized solar geoengineering moderates key climate hazards. *Nat Clim Change* 9(4):295–299. <https://doi.org/10.1038/s41558-019-0398-8>
- Jiang D, Tian Z, Lang X (2015) Mid-Holocene global monsoon area and precipitation from PMIP simulations. *Clim Dyn* 44:2493–2512. <https://doi.org/10.1007/s00382-014-2175-8>
- Jin X, Cao L, Zhang J (2022) Effects of solar radiation modification on the ocean carbon cycle: an earth system modeling study. *Atmos Ocean Sci Lett*. <https://doi.org/10.1016/j.aosl.2022.100187>
- Katzenberger A, Schewe J, Pongratz J, Levermann A (2021) Robust increase of Indian monsoon rainfall and its variability under future warming in CMIP6 models. *Earth Syst Dyn* 12(2):367–386. <https://doi.org/10.5194/esd-12-367-2021>
- Keith DW, Dowlatabadi H (1992) A serious look at geoengineering. *EOS Trans Am Geophys Union* 73(27):292–293
- Keith DW, Parson E, Morgan MG (2010) Research on global sun block needed now. *Nature* 463(7280):426–427. <https://doi.org/10.1038/463426a>
- Kravitz B, MacMartin DG (2020) Uncertainty and the basis for confidence in solar geoengineering research. *Nat Rev Earth Environ* 1:64–75. <https://doi.org/10.1038/s43017-019-0004-7>
- Kravitz B, MacMartin DG, Mills MJ, Richter JH, Tilmes S, Lamarque J, Vitt F (2017) First simulations of designing stratospheric sulfate aerosol geoengineering to meet multiple simultaneous climate objectives. *J Geophys Res Atmos* 122(23):12616–12634. <https://doi.org/10.1002/2017JD026874>
- Kravitz B, MacMartin DG, Tilmes S, Richter JH, Mills MJ, Cheng W, Vitt F (2019) Comparing surface and stratospheric impacts of geoengineering with different SO₂ injection strategies. *J Geophys Res Atmos* 124(14):7900–7918. <https://doi.org/10.1029/2019JD030329>
- Krishnamohan KS, Bala G (2022) Sensitivity of tropical monsoon precipitation to the latitude of stratospheric aerosol injections. *Clim Dyn* 59:151–168. <https://doi.org/10.1007/s00382-021-06121-z>
- Krishnamohan KS, Bala G, Cao L et al (2019) Climate system response to stratospheric sulfate aerosols: sensitivity to altitude of aerosol layer. *Earth Syst Dyn* 10:885–900. <https://doi.org/10.5194/esd-10-885-2019>
- Krishnamohan KS, Bala G, Cao L, Duan L, Caldeira K (2020) The climatic effects of hygroscopic growth of sulfate aerosols in the stratosphere. *Earths Future*. <https://doi.org/10.1029/2019EF001326>
- Krishnamohan KS, Modak A, Bala G (2021) Effects of local and remote black carbon aerosols on summer monsoon precipitation over India. *Environ Res Commun*. <https://doi.org/10.1088/2515-7620/AC18D1>
- Liu F, Chai J, Wang B, Liu J, Zhang X, Wang Z (2016) Global monsoon precipitation responses to large volcanic eruptions. *Sci Rep* 6(March):1–11. <https://doi.org/10.1038/srep24331>
- Liu F, Lu J, Garuba O, Ruby Leung L, Luo Y, Wan X (2018) The sensitivity of surface temperature to oceanic forcing via q-flux Green's function experiments. Part II: feedback decomposition and polar amplification. *J Clim* 31:6745–6761
- Lu J, Xue D, Leung LR, Liu F, Song F, Harrop B, Zhou W (2021) The leading modes of Asian summer monsoon variability as pulses of atmospheric energy flow. *Geophys Res Lett* 48:e2020. <https://doi.org/10.1029/2020GL091629>
- Lutsko NJ, Seeley JT, Keith DW (2020) Estimating impacts and trade-offs in solar geoengineering scenarios with a moist energy balance model. *Geophys Res Lett* 47(9):1–12. <https://doi.org/10.1029/2020GL087290>
- MacMartin DG, Kravitz B, Tilmes S, Richter JH, Mills MJ, Lamarque JF, Tribbia JJ, Vitt F (2017) The climate response to stratospheric aerosol geoengineering can be tailored using multiple injection locations. *J Geophys Res Atmos* 122(12):574–590. <https://doi.org/10.1002/2017JD026868>
- Mahajan A, Tingley D, Wagner G (2019) Fast, cheap, and imperfect? US Public Opin Sol Geoeng 28(3):523–543. <https://doi.org/10.1080/09644016.2018.1479101>
- Michael R (2003) Uncertainties and graphing. <http://spiff.rit.edu/classes/phys311/workshops/w1b/w1b.html>. Accessed July 2022
- Modak A, Bala G (2014) Sensitivity of simulated climate to latitudinal distribution of solar insolation reduction in solar radiation management. *Atmos Chem Phys* 14:7769–7779. <https://doi.org/10.5194/acp-14-7769-2014>
- Modak A, Bala G, Caldeira K et al (2018) Does shortwave absorption by methane influence its effectiveness? *Clim Dyn* 51:3653–3672. <https://doi.org/10.1007/s00382-018-4102-x>
- Mooley DA, Parthasarathy B (1984) Fluctuations in all-India summer monsoon rainfall during 1871–1978. *Clim Change* 6:287–301. <https://doi.org/10.1007/BF00142477>
- Myhre G, Myhre CEL, Samset BH, Storelvmo T (2013) Aerosols and their relation to global climate and climate sensitivity. *Nat Educ Knowl* 4:7
- Neale RB, Richter JH, Conley AJ, Park S, Lauritzen PH, Gettelman A, Williamson DL, Rasch, PJ, Vavrus SJ, Taylor MA, Collins WD, Zhang M, Lin S (2010) Description of the NCAR Community Atmosphere Model (CAM 4.0). NCAR Tech. Note NCAR/TN-485+STR, National Center for Atmospheric Research, Boulder, Colorado, USA
- Nalam A, Bala G, Modak A (2018) Effects of Arctic geoengineering on precipitation in the tropical monsoon regions. *Clim Dyn* 50:3375–3395. <https://doi.org/10.1007/s00382-017-3810-y>
- Oleson KW, Lawrence DM, Bonan GB et al (2010) Technical description of version 4.0 of the community land model (CLM). NCAR TECHNICAL NOTE
- Ramanathan V, Chung C, Kim D, Bettge T, Buja L, Kiehl JT, Washington WM, Fu Q, Sikka DR, Wild M (2005) Atmospheric brown clouds: impacts on South Asian climate and hydrological cycle. *Proc Natl Acad Sci USA* 102:5326–5333
- Rasch PJ, Crutzen PJ, Coleman DB (2008) Exploring the geoengineering of climate using stratospheric sulfate aerosols: the role of particle size. *Geophys Res Lett* 35(2):1–6. <https://doi.org/10.1029/2007GL032179>
- Richter JH, Tilmes S, Glanville A, Kravitz B, MacMartin DG, Mills MJ, Lamarque J-F (2018) Stratospheric response in the first geoengineering simulation meeting multiple surface climate objectives. *J Geophys Res Atmos* 123(11):5762–5782. <https://doi.org/10.1029/2018JD028285>
- Robock A, Oman L, Stenchikov GL (2008) Regional climate responses to geoengineering with tropical and Arctic SO₂ injections. *J Geophys Res Atmos* 113(16):1–15. <https://doi.org/10.1029/2008JD010050>

- Roose S, Joseph PV, Mohanakumar K (2019) Changes in the temperature distribution in the top 150 m of the equatorial Indian Ocean in association with El Niño and monsoon drought. *Int J Climatol* 39:31–42. <https://doi.org/10.1002/joc.5778>
- Rose BEJ, Rayborn L (2016) The effects of ocean heat uptake on transient climate sensitivity. *Curr Clim Change Rep* 2:190–201. <https://doi.org/10.1007/s40641-016-0048-4>
- Schneider T, Bischoff T, Haug GH (2014) Migrations and dynamics of the intertropical convergence zone. *Nature* 513(7516):45–53. <https://doi.org/10.1038/nature13636>
- Sherman P, Gao M, Song S, Archibald AT, Abraham NL, Lamarque J-F, Shindell D, Faluvegi G, McElroy MB (2021) Sensitivity of modeled Indian monsoon to Chinese and Indian aerosol emissions. *Atmos Chem Phys* 21:3593–3605. <https://doi.org/10.5194/acp-21-3593-2021>
- Simpson IR, Tilmes S, Richter JH, Kravitz B, MacMartin DG, Mills MJ, Pendergrass AG (2019) The regional hydroclimate response to stratospheric sulfate geoengineering and the role of stratospheric heating. *J Geophys Res Atmos* 124(23):12587–12616. <https://doi.org/10.1029/2019JD031093>
- Smith SJ, Van Aardenne J, Klimont Z, Andres RJ, Volke A, Delgado Arias S (2011) Anthropogenic sulfur dioxide emissions: 1850–2005. *Atmos Chem Phys* 11(3):1101–1116. <https://doi.org/10.5194/acp-11-1101-2011>
- Smyth JE, Russotto RD, Storelvmo T (2017) Thermodynamic and dynamic responses of the hydrological cycle to solar dimming. *Atmos Chem Phys* 17(10):6439–6453. <https://doi.org/10.5194/acp-17-6439-2017>
- Stenchikov GL, Kirchner I, Robock A, Graf HF, Antuña JC, Grainger RG, Thomason L (1998) Radiative forcing from the 1991 Mount Pinatubo volcanic eruption. *J Geophys Res Atmos* 103(D12):13837–13857. <https://doi.org/10.1029/98JD00693>
- Stuecker MF, Bitz CM, Armour KC, Proistosescu C, Kang SM, Xie S-P et al (2018) Polar amplification dominated by local forcing and feedbacks. *Nat Clim Chang* 8(12):1076–1081. <https://doi.org/10.1038/s41558-018-0339-y>
- Sun W, Wang B, Zhang Q, Pausata FSR, Chen D, Lu G et al (2019) Northern Hemisphere land monsoon precipitation increased by the Green Sahara during middle Holocene. *Geophys Res Lett* 46:9870–9879. <https://doi.org/10.1029/2019GL082116>
- Svoboda T, Keller K, Goes M, Tuana N (2011) Sulfate aerosol geoengineering: the question of justice. *Public Aff Q* 25(3): 157–179. <http://www.jstor.org/stable/23057076>
- Tilmes S, Fasullo J, Lamarque JF et al (2013) The hydrological impact of geoengineering in the Geoengineering Model Intercomparison Project (GeoMIP). *J Geophys Res Atmos* 118:1111–3658. <https://doi.org/10.1002/jgrd.50868>
- Tilmes S, Richter JH, Mills MJ, Kravitz B, Macmartin DG, Vitt F, Lamarque JF (2017) Sensitivity of aerosol distribution and climate response to stratospheric SO₂ injection locations. *J Geophys Res Atmos* 122(23):12591–12615. <https://doi.org/10.1002/2017JD026888>
- Tilmes S, Richter JH, Kravitz B, Macmartin DG, Mills MJ, Simpson IR, Ghosh S (2018) CESM1(WACCM) stratospheric aerosol geoengineering large ensemble project. *Bull Am Meteorol Soc* 99(11):2361–2371. <https://doi.org/10.1175/BAMS-D-17-0267.1>
- Tilmes S, MacMartin GD, Lenaerts TM, Van Kampenhout J, Muntjewerf L, Xia L, Robock A (2020) Reaching 1.5 and 2.0°C global surface temperature targets using stratospheric aerosol geoengineering. *Earth Syst Dyn* 11(3):579–601. <https://doi.org/10.5194/esd-11-579-2020>
- Turner A, Annamalai H (2012) Climate change and the South Asian summer monsoon. *Nat Clim Change* 2:587–595. <https://doi.org/10.1038/nclimate1495>
- Visioni D, Pitari G, di Genova G, Tilmes S, Cionni I (2018) Upper tropospheric ice sensitivity to sulfate geoengineering. *Atmos Chem Phys* 18(20):14867–14887. <https://doi.org/10.5194/acp-18-14867-2018>
- Visioni D, MacMartin DG, Kravitz B, Tilmes S, Mills MJ, Richter JH, Boudreau MP (2019) Seasonal injection strategies for stratospheric aerosol geoengineering. *Geophys Res Lett* 46(13):7790–7799. <https://doi.org/10.1029/2019GL083680>
- Visioni D, MacMartin DG, Kravitz B, Richter JH, Tilmes S, Mills MJ (2020) Seasonally modulated stratospheric aerosol geoengineering alters the climate outcomes. *Geophys Res Lett* 47(12):1–10. <https://doi.org/10.1029/2020GL088337>
- Wang C (2004) A modeling study on the climate impacts of black carbon aerosols. *J Geophys Res* 109(D3):D03106. <https://doi.org/10.1029/2003JD004084>
- Wang B, Ding Q (2006) Changes in global monsoon precipitation over the past 56 years. *Geophys Res Lett* 33:1–4. <https://doi.org/10.1029/2005GL025347>
- Wang B, Lin H (2002) Rainy season of the asian–pacific summer monsoon. *J Clim* 15(4):386–398. [https://doi.org/10.1175/1520-0442\(2002\)015\(0386:RSOTAP\)2.0.CO;2](https://doi.org/10.1175/1520-0442(2002)015(0386:RSOTAP)2.0.CO;2)
- Wang B, Jin C, Liu J (2020) Understanding future change of global monsoons projected by CMIP6 models. *J Clim* 33(15):6471–6489. <https://doi.org/10.1175/JCLI-D-19-0993.1>
- Wigley TML (2006) A combined mitigation/geoengineering approach to climate stabilization. *Science* 314:452–454. <https://doi.org/10.1126/science.1131728>
- Zhao Y, Harrison SP (2012) Mid-Holocene monsoons: a multi-model analysis of the inter-hemispheric differences in the responses to orbital forcing and ocean feedbacks. *Clim Dyn* 39:1457–1487. <https://doi.org/10.1007/s00382-011-1193-z>
- Zhao M, Cao L, Bala G, Duan L (2021) Climate response to latitudinal and altitudinal distribution of stratospheric sulfate aerosols. *J Geophys Res Atmos* 126:1–19. <https://doi.org/10.1029/2021jd035379>

Publisher's Note Springer Nature remains neutral with regard to jurisdictional claims in published maps and institutional affiliations.